Variable-Angle Time-Resolved Evanescent Wave-Induced Fluorescence Spectroscopy (VATR-EWIFS): A Technique for Concentration Profiling Fluorophores at Dielectric Interfaces

Christopher D. Byrne,[†] Andrew J. de Mello,*[,†] and William L. Barnes[‡]

Zeneca/SmithKline Beecham Centre for Analytical Sciences, Department of Chemistry, Imperial College of Science, Technology and Medicine, Exhibition Road, London SW7 2AY, U.K., and Department of Physics, University of Exeter, Stocker Road, Exeter, EX4 4QL, U.K.

Received: July 28, 1998; In Final Form: September 15, 1998

The concentration distributions of fluorescein and acridine orange, at a water/silica interface, are determined using the technique variable-angle time-resolved evanescent wave-induced fluorescence spectroscopy. It is demonstrated theoretically that the radiative fluorescence lifetime of a molecule is affected in only a minor way by the presence of a dielectric interface. Consequently, time-resolved evanescent wave-induced fluorescence spectroscopy is used to measure the variations in the fluorescence quantum yield caused by the pressence of the interface. Knowledge of these variations is then used to determine molecular concentration distributions. The concentration distribution of fluorescein is found to be uniform and homogeneous as a function of distance away from the hydrophilic silica surface. However, it is found that a water/silica interface has a definite affect on the concentration distribution of acridine orange. A "surface associated" acridine orange population distinguishable from "bulk" acridine orange is demonstrated by spectral and kinetic analysis of EWIF emission. This information is then used to create concentration profiles of both molecular populations.

Introduction

Fluorescence spectroscopy is a highly sensitive analytical technique and is routinely used in the physical, biological, and chemical sciences to probe the structure, conformation, dynamics, and environment of atomic and molecular species. It is unique among spectroscopic techniques due to its inherent multidimensionality.[1] More specifically, the process of emission yields a diversity of orthogonal information that is intrinsically related to the nature of the fluorophore and its immediate environment.[2]

Much attention has been focused on the study of molecular interactions and dynamics at interfaces.[3,4] This is primarily due to their fundamental importance in many areas of chemistry and physics. One technique that has been successfully used to probe interfacial phenomena is evanescent wave-induced fluorescence spectroscopy (EWIFS).[5−10] EWIFS utilizes total internal reflection geometry to generate a surface-specific, electromagnetic field disturbance at the interface between two dielectric media.[11] EWIFS has been used to characterize the interfacial characteristics of many species, ranging from small dye molecules to macromolecules such as proteins, polymers, enzymes, and DNA.[12−16] The surface specificity of the evanescent wave has also been successfully used in many biosensing applications.[17,18] If receptor molecules are immobilized onto a dielectric surface, evanescent waves allow the investigation of ligand−receptor interactions without any perturbing separation or preconcentration steps.

Although fluorescence spectroscopy offers exquisite sensitivity, care must be taken when using it as a quantitative tool. Variations in fluorescence intensities are not only caused by changes in molecular concentrations but also by variations in the rates of radiative and nonradiative relaxation processes.[19] Changes in the local environment of a fluorophore can have a large affect on the nature of these processes and thus give rise to variations in the spectral and kinetic character of the emission. It has been demonstrated that these effects are particularly significant in heterogeneous environments such as the "interface".[5,6]

In this paper we address the idea that variations in the radiative rate coefficient, k_r, at a solid/liquid interface do not adversely affect the use of EWIFS as a quantitative interfacial probe. Consequently, the concentration distributions of two small dye molecules (fluorescein and acridine orange) in the interfacial region are elucidated, through measurement of both time-integrated and time-resolved fluorescence data.

Theory

When a molecule absorbs light, it is raised in energy to an excited state. From this excited state the molecule may relax back down to a ground state by emitting a photon (a radiative transition) or by dissipating energy in some other way (a nonradiative transition). The fluorescence quantum yield, ϕ_f, defines the fraction of excited-state species that become deexcited by fluorescence (singlet−singlet transitions) and is given by eq 1, where k_r and $\sum k_{nr}$ are the radiative and sum of the

$$\phi_f = \frac{k_r}{k_r + \sum k_{nr}} \tag{1}$$

nonradiative rate coefficients, respectively. Since the fluorescence quantum yield describes the fraction of the absorbed energy that is re-emitted as photons, the following expression can be written:

$$I_f = \phi_f I_a c \tag{2}$$

* To whom correspondence should be sent.
[†] Imperial College of Science, Technology and Medicine.
[‡] University of Exeter.

10.1021/jp983200u CCC: $15.00
Published on Web 11/13/1998

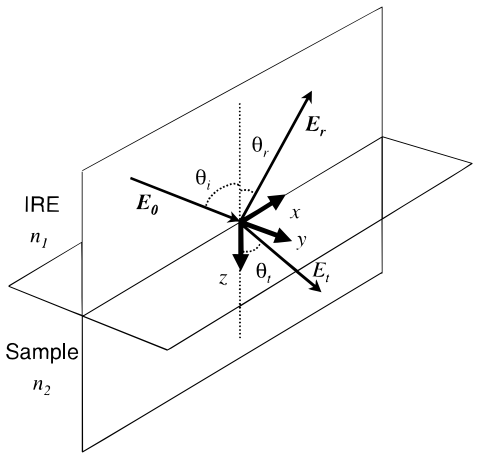

Figure 1. Coordinate system for VATR-EWIFS. A plane electromagnetic wave strikes the interface between medium 1 (the internal reflection element) and medium 2 (the sample at an angle of incidence, θ_i).

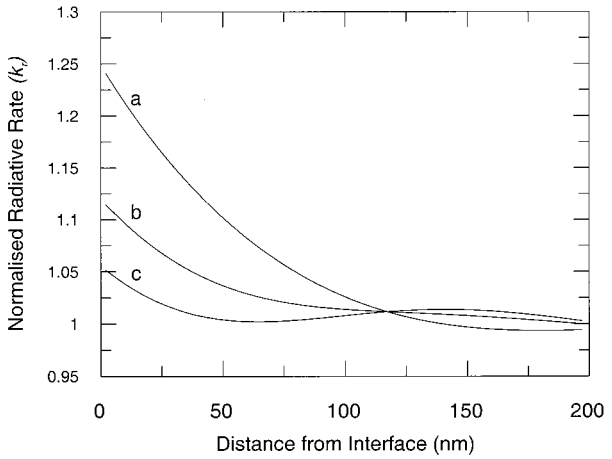

Figure 2. Calculated decay rate as a function of distance between the fluorophore and the interface, assuming the fluorescence quantum yield is 1.0. The rate is normalized with respect to that in the absence of the interface. Data are shown for dipole moments perpendicular to the interface (a), parallel to the interface (c), and for an isotropic distribution (b).

Here c is the concentration of fluorophores in a sample, I_a is the intensity of the light absorbed by the sample, and I_f is the intensity of the subsequent emission. If the fluorescence quantum yield is invariant of concentration, time-integrated fluorescence emission intensities can be directly related to molecular concentrations. However, such an assumption is often ill-conditioned since changes in fluorescence intensities are frequently due to variations in molecular relaxation rates (which in turn alter ϕ_f). This situation is particularly true in heterogeneous environments such as the interfacial region.[5−7] Consequently, variations in molecular concentrations inferred from fluorescence intensity changes must be treated with caution. Fluorescence quantum yields can be estimated through a kinetic analysis of the emission process, i.e., measuring the molecular fluorescence lifetime, since,

$$\phi_f = k_r \tau_f \tag{3}$$

where τ_f is the fluorescence lifetime. If k_r is assumed constant, then changes in ϕ_f can be evidenced by variations in the measured fluorescence lifetime. Unfortunately, the decay rate of a fluorophore may be modified by the presence of an interface.[20] This is an obvious concern in EWIFS measurements as variations in k_r prevent the application of EWIFS to quantitative problems. Variations in k_r occur because of interfacial electromagnetic boundary conditions imposed on the radiating field of a dipole.[21,22] This is primarily because the interface reflects the radiating field produced by a fluorophore. If a fluorophore is considered to be a forced, damped oscillating electric dipole, it can be seen that the field reflected by the interface provides the driving term with both the amplitude and phase of the reflected wave being important. The relative phase of the reflected and source fields depends not only on the phase change on reflection but also on the distance between the fluorophore and the interface. If the reflection returns to the fluorophore in phase, then emission will be enhanced and the decay rate will rise; if it returns out of phase, emission is inhibited and the rate will fall. The amplitude of the reflected wave is also important, since the stronger the reflection, the greater the potential for modification to the rate. Figure 1 shows the coordinate system for a conventional experiment. For the current experiments, the refractive index difference of fused silica/water interface is small ($n_{silica} = 1.46$, $n_{water} = 1.33$).

The affect of the interface on the decay rate has been modeled classically by many authors,[23−25] and the results of such calculations have been well-verified experimentally.[25] The modification to the decay rate is found to be dependent on the orientation of the electric dipole moment of the fluorophore with respect to the plane of the interface, the two unique orientations being perpendicular (subscript ⊥) and parallel (subscript ||) to the plane. The decay rates for these two orientations are found to be[25]

$$b_{\perp,||} = b_0(1 - \phi_f z_{\perp,||}) \tag{4}$$

The parameters $z_\perp$ and $z_{||}$ are given by

$$z_\perp = 1 - \frac{3}{2}\,\mathrm{Im}\int_0^\infty \frac{u^3}{l_1}(1 - r^p_{1,2})e^{-i\beta}\,du \tag{5}$$

$$z_{||} = 1 - \frac{3}{4}\,\mathrm{Im}\int_0^\infty \frac{u}{l_1}[(1 + r^s_{1,2}) - (1 - u^2)(1 + r^p_{1,2})]e^{-i\beta}\,du \tag{6}$$

The variable of integration, u, is the component of the wavevector (of the dipole field) in the plane of the interface, normalized with respect to the far field wavevector k_1 of the dipole radiation field in medium 1 (in this case the water); thus, $u = k_x/k_1$. The parameter l_1 is given by $l_1 = -i(1 - u^2)^{1/2}$ and is related to the component of the wavevector perpendicular to the interface. The phase angle β is the phase due to retardation, i.e., the phase change incurred in the round trip from the fluorophore, to the interface and back. The coefficients $r^p_{1,2}$ and $r^s_{1,2}$ are the Fresnel reflection coefficients for p and s polarized light at the interface, respectively, evaluated as a function of u.[25] Since the latter may range over all positive values between 0 and ∞, the reflection coefficients have to be calculated for both real and complex angles of incidence, corresponding to incident waves that are propagating and evanescent (this is in contrast to eq 9 below where the angles are always real).

Equation 4 is used to model the change in the decay rate, k_r, for two different values of the fluorescence quantum yield, 1.0 and 0.1. The results of such calculations, made as a function of distance between the fluorophore and the interface, are shown in Figure 2 and Figure 3. Results are shown for the two dipole orientations. Also shown are the results for an isotropic distribution of dipole orientations (a dipole whose moment

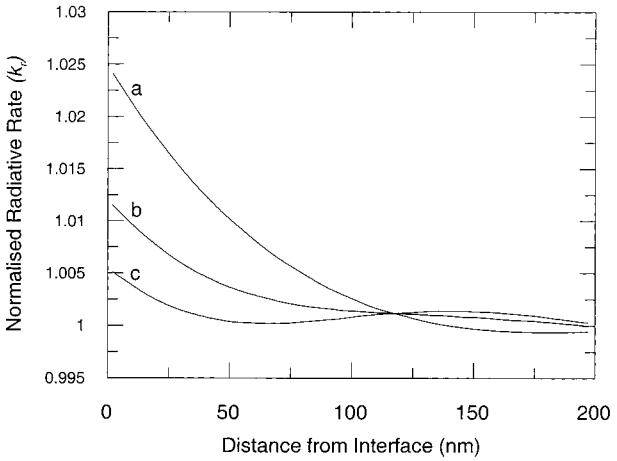

Figure 3. Calculated decay rate as a function of distance between the fluorophore and the interface, assuming the fluorescence quantum yield is 0.1. The rate is normalized with respect to that in the absence of the interface. Data are shown for dipole moments perpendicular to the interface (a), parallel to the interface (c), and for an isotropic distribution (b).

rotates and samples all directions in space in a time much faster than the fluorescence lifetime). In this case, the decay rate b_{iso} is given by

$$b_{iso} = {}^2/_3 b_{||} + {}^1/_3 b_{\perp} \tag{7}$$

We note that the dominant effect of the interface is to increase the radiative rate for fluorophores close (<100 nm) to the interface. However, the changes are small, as anticipated above, becoming less important as the fluorescence quantum yield falls. Consequently, in most EWIFS measurements it is valid to relate changes in fluorescence lifetime to changes in fluorescence quantum yield.

In EWIFS light strikes the interface between two media of differing refractive indices. If the light is traveling in the optically dense medium (refractive index $= n_1$) and is incident at the interface at an angle, θ_i, greater than the critical angle, it will undergo total internal refection. Under these conditions an evanescent wave is established in the rarer medium (refractive index, n_2).[11] When medium 2 is absorbing, its refractive index becomes complex and is given by the following:

$$n_2 = n_2(1 + i\kappa) \tag{8}$$

Here κ is an extinction coefficient that is related to the absorption index of the sample. The properties of the evanescent wave can be calculated from Maxwell's equations by assuming the electric field across the interface is continuous (the case for perpendicular polarized light shall be considered here).[26] Boundary conditions mean that the intensity of the electromagnetic radiation at the interface, but in medium 2, is given by the expression[27]

$$I_0 = \mathbf{E}_0{}^2 \frac{4{n_1}^2 \cos^2\theta_i}{(n_1 \cos\theta_i + \mathrm{Re})^2 + \mathrm{Im}^2} \exp\left(-\frac{4\pi(\mathrm{Im})z}{\lambda_0}\right) \tag{9}$$

where $\mathbf{E}_0$ is the electric field amplitude of the incident wave, λ_0 is the wavelength of the incident light, θ_i is the angle of incidence, and Re and Im are the real and imaginary parts of the refractive index and are defined as

$$\mathrm{Re} = ([{n_2}^2(1-\kappa^2) - {n_1}^2 \sin^2\theta_i + \{[{n_2}^2(1-\kappa^2) - {n_1}^2 \sin^2\theta_i]^2 + 4{n_2}^4\kappa^2\}^{1/2}]/2)^{1/2} \tag{10}$$

$$\mathrm{Im} = ([-{n_2}^2(1-\kappa^2) + {n_1}^2 \sin^2\theta_i + \{[{n_2}^2(1-\kappa^2) - {n_1}^2 \sin^2\theta_i]^2 + 4{n_2}^4\kappa^2\}^{1/2}]/2)^{1/2} \tag{11}$$

The implication of these boundary conditions is that for total internal reflection there exists an electromagnetic disturbance in the rarer medium. This disturbance is termed an evanescent wave. Equation 9 shows that its amplitude decreases exponentially with distance from the interface. A characteristic (but arbitrary) penetration depth, d_p, of the evanescent wave is commonly given by eq 12. This defines the distance into the rarer medium when the electric field amplitude of the evanescent wave is 1/e of its interfacial value.

$$d_p = \frac{\lambda_0}{2\pi\mathrm{Im}} \tag{12}$$

In the EWIF experiment the total emitted fluorescence intensity I_f can be derived from eq 2 and is the integrated product of the evanescent wave energy, the molecular fluorescence quantum yield profile, and concentration profile. If the observation angle is assumed to be zero,[7,27]

$$I_f(\theta_i, z) = \int_0^\infty \phi_f(z) c(z) I_0 \exp(-z/d_p)\, dz \tag{13}$$

In a simple case where the fluorophore is not effected by the surface, $\phi_f(z)$ and $c(z)$ can be assumed to be constant over all z. For this to be valid spectral and kinetic properties of the fluorescence emission must be invariant and independent of incidence angle and penetration depth. Under these conditions eq 13 becomes

$$I_f(\theta_i) \propto \frac{4{n_1}^2 \cos^2\theta_i}{(n_1 \cos\theta_i + \mathrm{Re})^2 + \mathrm{Im}^2} \frac{\lambda_0}{4\pi\mathrm{Im}} \tag{14}$$

Consequently if the fluorophore is completely uneffected by the presence of the interface and fluorescence intensity is measured as a function of incidence angle eq 14 can be used to model experimentally obtained data.[7,27] Unfortunately heterogeneous interfacial environments may affect the physical and photophysical properties a fluorophore. A molecule that interacts with the surface may give rise to nonuniform concentration and fluorescence quantum yield distributions in the interfacial region that are unlikely to be invariant of distance from the interface; thus, all terms in eq 13 need to be evaluated. The step function is a simple mathematical model that can be used to describe basic distributions of $c(z)$ and $\phi(z)$. Step functions presuppose that fluorescence originates from two distinct layers of variable thickness, one associated with the surface and the other associated with the bulk solution. Assuming that the intensity of the emitted fluorescence is proportional to the product of the molecular concentration and the fluorescence quantum yield, the step function is expressed as

$$c(z)\phi_f(z) = \sigma_1 \quad z \le r \tag{15}$$

$$c(z)\phi_f(z) = \sigma_2 \quad z > r \tag{16}$$

where σ_1 and σ_2 are the relative emissivities of the interfacial and the bulk layers respectively and r is the thickness of the interfacial layer. Substituting the step function into eq 13 and

solving with an inverse Laplace transform,[28,29] one can show that the fluorescence intensity varies with incidence angle as follows:

$$I_f(z,\theta) = \frac{4{n_1}^2 \cos^2 \theta_i}{(n_1 \cos \theta_i + \mathrm{Re})^2 + \mathrm{Im}^2} \times [\sigma_1 d_p(1 - e^{(-r/d_p)}) + \sigma_2 d_p e^{(-r/d_p)}] \quad (17)$$

If it is suspected that a fluorophore interacts with the interface, then eq 17 can be used to model angle spectra to produce an emissivity depth distribution. The emissivity depth distribution can then be combined with fluorescence quantum yield information obtained from time-resolved EWIFS to produce a concentration depth profile of fluorophores in the interfacial region.

Experimental Section

Fluorescein disodium salt (FDSS, ICN Biomedical) and acridine orange (A0, Sigma) were used as received. All aqueous solutions were made up using distilled deionized water (18.2 MΩ, Elga, Maxima). Concentrations were determined from absorbance measurements using an extinction coefficient, ϵ_{max} of 8.8×10^4 M^{-1} cm^{-1} for FDSS and 5.3×10^4 M^{-1} cm^{-1} for AO.

Excitation light was provided by a cavity-dumped Argon ion laser (Lexel 95). This produced a 5 MHz pulse train (fwhm ≈ 7 ns) at 488 nm. The output power was kept below 1 mW to avoid photobleaching of the sample. Excitation laser pulses were perpendicularly polarized with respect to the plane interface. The internal reflection element used for all EWIFS experiments was a fused silica dove prism ($n_1 = 1.46$). Fluorescence was collected perpendicular to the surface, through the internal reflection element using a high numerical aperture lens. Fluorescence was focused on to the slits of a scanning 0.22 m single monochromator (Spex 1681). Entrance and exit slits were set to produce a 2 nm band-pass. All fluorescence measurements were made using the technique of single-photon counting. Time-integrated measurements were made using a single-photon counting system consisting of a photomultiplier (Hamamatsu, R6358P) and a gated photon counter (Stanford Research Systems, SR400) interfaced to a personal computer. Fluorescence decays were obtained using a time-correlated single-photon counting (TCSPC[30]) system consisting of a constant fraction discriminator (Ortec 584), a time-to-amplitude converter (Ortec 437A), and multichannel analyzer (Oxford Instruments, PCAIII PC card). Fluorescence decays were collected to at least 10 000 counts in the channel of maximum intensity and were analyzed using a sum of exponential (SOE) iterative reconvolution fitting routine based on the Marquardt−Levenberg algorithm.[31]

For depth-resolved EWIF experiments the internal reflection element and detection system remained fixed. Variations in the incidence angle were effected using a rotating mirror mounted on a translation stage. Computer-controlled stepper motors (Physik Instumente, C-560) on the translation and rotation stages ensure that the position of the evanescent wave remains constant through the experiment.

The prism surface was cleaned prior to every experiment using the following procedure. The surface of the prism is washed for 1 min in copious amounts of distilled/deionized water and dried using N_2. The entire prism is then immersed in CrO_2/H_2SO_4 at 70 °C and soaked for 1 h. It is then removed from the acid and rinsed with deionized water. Before the surface is dry, the prism is placed on the flow cell and contacted with solvent only, followed by sample and solvent. Although no specific characterization of water contact angles was performed, the aggressive cleaning procedure produced what was considered a consistent "hydrophilic" surface.

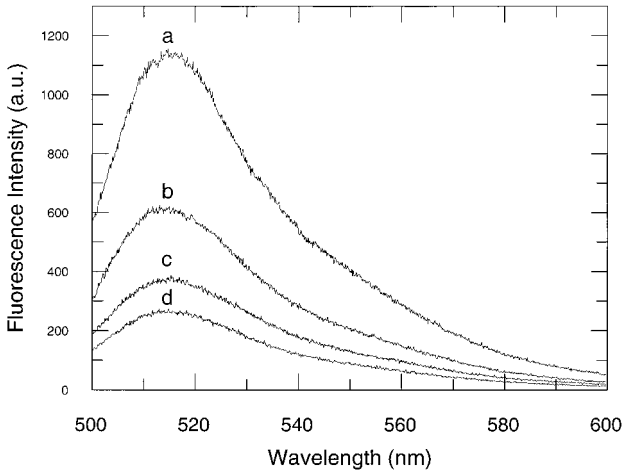

Figure 4. EWIF emission spectra of FDSS at the water/silica interface. Bulk solution concentration = 7.2×10^{-6} mol dm^{-3}; θ_i = (a) 65.0°, (b) 66.2°, (c) 68.0°, and (d) 80.0°.

Results and Discussion

Fluorescein. Figure 4 shows EWIF emission spectra of FDSS collected at four different internal reflection angles. At incidence angles of 80 and 68° the evanescent wave only interrogates FDSS molecules ($d_p \approx 100$ nm). Below the critical angle, at incidence angles of 66.8 and 65°, the depth of penetration is much larger ($d_p \approx 100$ μm); consequently both surface and bulk species are interrogated.

As the angle of incidence is decreased, the fluorescence intensity is seen to increase. This in part, is due to the increase in the depth of penetration as the incidence angle is reduced. At extended penetration depths larger sample volumes are excited and consequently the measured fluorescence intensity increases. Importantly the spectral profile is identical at all incidence angles (emission spectra are also identical to bulk fluorescence emission spectra collected using conventional right angle geometries). It can be concluded that the spectral characteristics of the fluorescence emission of FDSS are uneffected by the presence of the hydrophilic fused silica surface. Subsequently, the kinetic characteristics of the fluorescence emission were also examined.

Figure 5 shows the fluorescence decay of FDSS in solution (a) alongside the EWIF decay of FDSS at a fused water/silica interface (b). Both decays are analyzed using a single-exponential decay function and yield excellent fits at all levels of precision ($\tau_f = 4.71$ ns, $\chi^2 < 1.2$). The observed lifetime is consistent with the reported literature value of 4.7 ns.[32] Additional EWIF decays were collected at incidence angles of 68, 66.8, and 65° ($\theta_c \approx 66.8°$). If fluorescence decays originate from a system containing a single species, then the decay times will be invariant of dataset. Global SOE analysis allows multiple datasets to be analyzed simultaneously, where a single lifetime is common to all datasets. The application of a model over a multidimensional data surface is statistically the most rigorous test of a particular a priori model that can be performed. If the model satisfies all the statistical parameters, then there is nothing more that can be done to test that particular model.[33] All six decays were analyzed using a single-exponential global model and the results are shown in Table 1. Table 1 shows

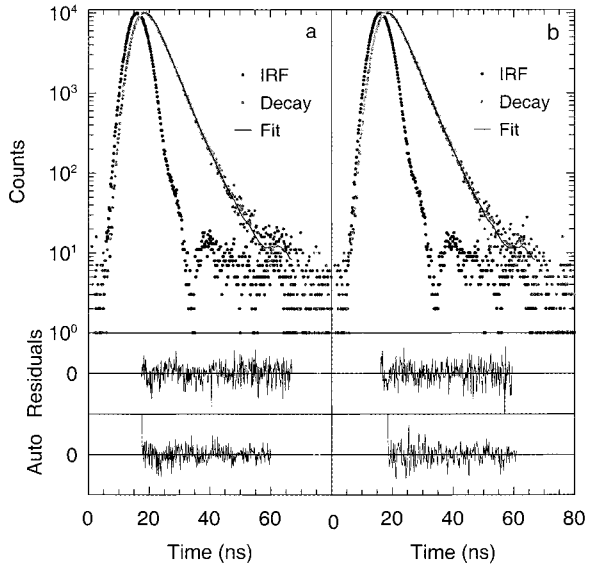

Figure 5. Fluorescence decay profiles of FDSS. Concentration = 7.2 × 10^{-7} mol dm^{-3} key: (a) free solution (τ_f = 4.7 ns); (b) silica/water interface (d_p = 100 nm) (τ_f = 4.7 ns). (Residuals and auto correlation functions are also shown.)

TABLE 1: Global SOE Analysis of Fluorescence Decay Profiles of FDSS at a Water/Silica Interface[a]

incidence angle	τ_f (ns)	χ^2	DW
80.0	4.7	1.34	1.73
68.0	4.7	1.27	1.89
66.8	4.7	1.31	1.62
65.0	4.7	1.27	1.89
bulk	4.7	1.39	1.91

[a] Bulk solution concentration = 7.2 × 10^{-6} mol dm^{-3}. Global χ^2 = 1.3.

that a single-exponential global model is an excellent description of all the data sets. This suggests that the fluorescence lifetime of FDSS is independent of its local environment. Identical results were found at all FDSS concentrations. If the radiative rate constant of a fluorophore is assumed to be uneffected by the interface, we can assume that the fluorescence quantum yield and hence the photophysical properties of FDSS are also unchanged by the presence of the hydrophilic silica surface. Importantly, this allows depth distributions obtained from the analysis of angle spectra to be related directly to concentration profiles.

Figure 6 shows the dependence of fluorescence intensity on incidence angle for various concentrations of FDSS at a water/silica interface. The solid curves represent the results of fitting the experimental data to eq 14 using a generalized reduced gradient (GRG) nonlinear optimization routine. There are three fitting parameters, the refractive index of medium 2, the extinction coefficient κ, and a proportionality constant. Statistically adequate fits are obtained for all data sets. At all FDSS concentrations the real part of the refractive index n_2 is constant at 1.336. The inset in Figure 6 shows κ versus concentration. The linearity between the extinction coefficient and the concentration of the FDSS solutions is of excellent quality. Excellent fits for all datasets (to eq 14) clearly indicates that FDSS has a homogeneous concentration depth distribution.

Acridine Orange. Figure 7 shows area normalized EWIF emission spectra of AO at a water/silica interface, collected at internal reflection angles of 80.0, 68.0, 66.8, and 65.0° (bulk solution concentration = 2.1 × 10^{-7} mol dm^{-3}). In much the same way as FDSS, the fluorescence intensity is observed to

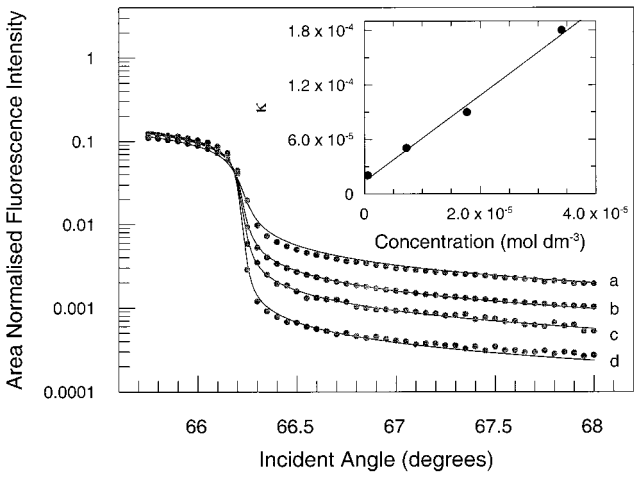

Figure 6. Angle spectra of FDSS at the water/silica interface. Concentration: (a) 3.4 × 10^{-5}; (b) 1.7 × 10^{-5}; (c) 7.2 × 10^{-6}; (d) 5.9 × 10^{-7} mol dm^{-3}. Inset: extinction coefficient resulting from fit of experimental data to eq 14 vs bulk solution concentration.

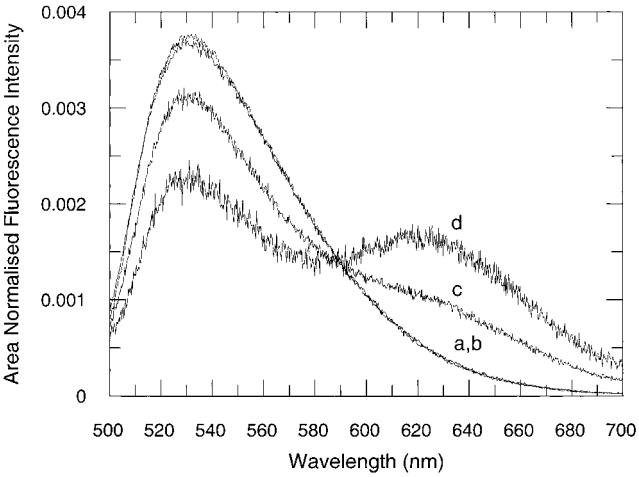

Figure 7. Area-normalized EWIFS emission spectra of acridine orange at the silica/water interface. Bulk solution concentration = 2.1 × 10^{-7} mol dm^{-3}; θ_i = (a) 65.0°, (b) 66.2°, (c) 68.0°, and (d) 80.0°.

increase as the incidence angle decreases. However, the spectral profile of the EWIFS emission changes dramatically as a function of incidence angle. At the shortest penetration depth ($d_p \approx$ 100 nm), emission has two distinct peaks (528 and 625 nm). As the penetration depth is increased, the relative intensity of the two emission peaks changes (the intensity of 528 nm peak increases relative to emission at 625 nm). As the incidence angle is lowered past the critical angle (θ_c = 66.8°), the penetration depth tends toward infinity and the emission shows only a single peak at 528 nm. These results demonstrate that the presence of the hydrophilic silica surface generates a population of "surface-associated" AO species that have a red shifted (≈100 nm) emission maximum with respect to the bulk solution species. The photophysical properties of this surface population are investigated further by examining the kinetic characteristics of emission.

Figure 8 shows fluorescence decay profiles of AO in solution and at a water/silica interface ($d_p \approx$ 100 nm) measured at two emission wavelengths. For AO in free solution analysis of the profiles using a single-exponential decay function produces excellent fits at all levels of precision (Figure 8a,b), τ_f = 2.1 ns, $\chi^2 < 1.1$). However for AO at the water/silica interface single exponential analysis of the decays produced very poor fits at all levels of precision. In light of this the complexity of

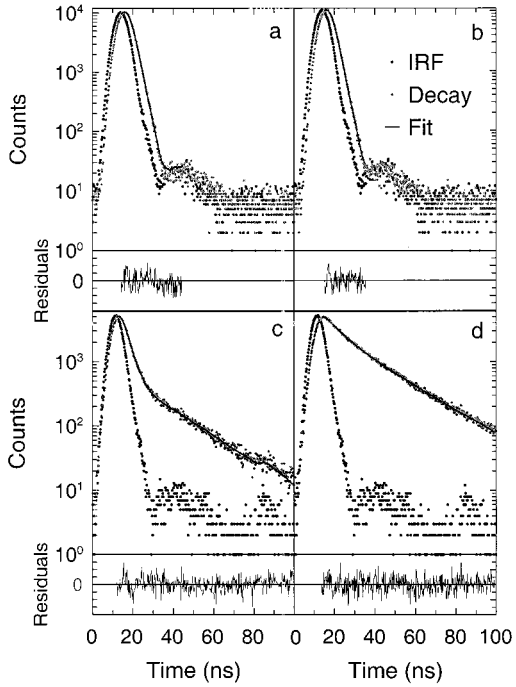

Figure 8. Fluorescence decay profiles of acridine orange. Bulk solution concentration = 2.1×10^{-7} mol dm^{-3}. In free solution, emission wavelength = (a) 550 nm and (b) 650 nm. At the water/silica interface (d_p = 100 nm), emission wavelength = (c) 550 nm and (d) 650 nm. Fluorescence lifetime analysis of AO decays is shown in Tables 2 and 3.

TABLE 2: SOE Fluorescence Lifetime Analysis of AO Decays, Where τ_1 and τ_2 Are the Recovered Lifetimes of the Two Decay Time Components and A_1 and A_2 Are the Percentage Amplitudes of the Two Decay Time Components

excitation	wavelength (nm)	τ_1	A_1	τ_2	A_2	χ^2	DW
bulk	550	2.1	100			1.12	1.62
bulk	650	2.1	100			1.18	1.78
EWIFS $\theta_i = 80^0$	550	2.2	78	24.5	22	1.24	1.62
EWIFS $\theta_i = 80^0$	650	2.0	24	25.3	76	1.19	1.52

TABLE 3: Global Sum of Exponential Analysis of AO Decays

excitation	wavelength (nm)	amplitude (%) $\tau_1 = 2.1$ ns	$\tau_2 = 24.3$ ns	χ^2	DW
bulk	550	100		1.14	1.89
bulk	650	100		1.18	1.73
EWIFS $\theta_i = 80^0$	550	72	28	1.24	1.57
EWIFS $\theta_i = 80^0$	650	16	84	1.33	1.76

the model was increased to include a second exponential term. The increase in the complexity is physically justified by the observed variations in the spectral characteristics (Figure 7). Analysis of the EWIF decays produced excellent fits to a biexponential model (Figure 8c,d). Table 2 shows the results of the SOE analysis of the four fluorescence decays. All the decays show a short lifetime component ($\tau_f \approx 2.1$ ns) that is characteristic of AO in free solution. The analysis also shows that decays from the interfacial region contain a second component with an increased lifetime ($\tau_f \approx 25$ ns). This suggests that the presence of the interface produces a second, surface-modified, AO species characterized by an increased florescence lifetime. To test this idea global SOE analysis, using a biexponential decay model, was performed on the four AO fluorescence decays. The results are shown in Table 3. As stated, global analysis is the most rigorous statistical test that

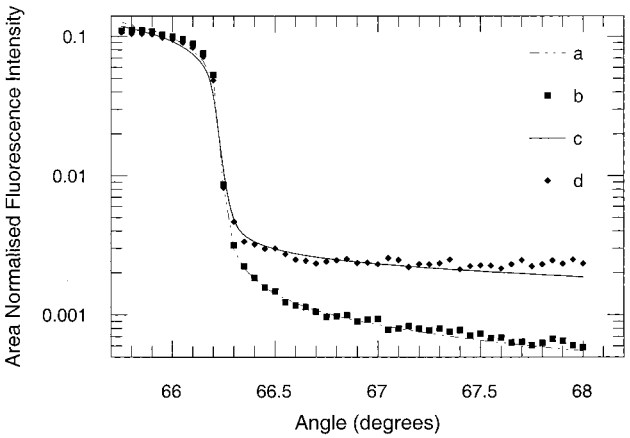

Figure 9. EWIF angle spectra of acridine orange. Bulk solution concentration = 2.1×10^{-7} mol dm^{-3}. Emission wavelength = (b) 550 nm and (d) 650 nm. Successful fits of experimental data to eq 17 are for (a) 550 nm and (d) 650 nm.

can be performed on the data and the excellent fits demonstrate that the two-component model is a good statistical description of the system.

The results of the fluorescence lifetime analysis demonstrate that in free solution AO exists as a single fluorescent species, characterized by a peak emission at 528 nm and fluorescence lifetime of 2.1 ns. The EWIFS decays suggest that in the interfacial region a modified AO population exists, characterized by red-shifted fluorescence emission (625 nm) and a hugely increased fluorescence lifetime ($\tau_f \approx 25$ ns). The large red shift in the emission of the "surface-associated" species allows simple discrimination between "surface-associated" and "bulk" AO. Consequently angle spectra of AO taken at different emission wavelengths were measured to probe depth distributions of the different populations. At longer wavelengths the depth distribution of surface specific species is preferentially investigated, whereas at shorter wavelengths bulk AO species are selectively probed. Figure 9 shows the angle spectra of AO measured at two different emission wavelengths, 550 and 650 nm. Above the critical angle the penetration depth of the evanescent wave is of the order of a few hundred nanometers. The two angle spectra are clearly very different in shape, indicating differences in the depth distributions of the two AO species. Below the critical angle both angle spectra are almost identical, since penetration depths are now of the order of a few hundred microns (i.e. for an emission wavelength of 650 nm the majority of the observed fluorescence originates from bulk AO species).

The two angle spectra were fitted to eq 17, using four fitting parameters, κ the extinction coefficient, n_2 the real part of the refractive index of medium two, r the thickness of the interfacial layer, and σ_1:σ_2 the relative concentration of the bulk and interfacial layers. Of these parameters κ and n_2 characterize the absorption properties of the system while r and σ_1:σ_2 characterize the depth distribution of the system.

At both emission wavelengths the real part of the refractive index and the extinction coefficient resulting from the fits were identical ($n_2 = 1.336$ and $\kappa = 4 \times 10^{-5}$); this is expected as the optical absorption properties of the sample are not affected by the wavelength at which the fluorescence emission is monitored. Similarly the thickness of the interfacial layer r was also found to be independent of emission wavelength (≈40 nm). However, the resulting depth distributions at each emission wavelength are very different and are illustrated in Figure 10. The depth distribution of AO measured at 650 nm spectrally selects AO species associated with the surface. (The *y*-axes in

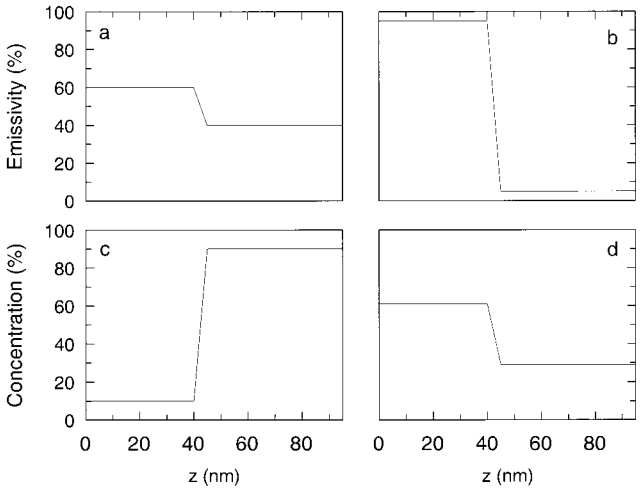

Figure 10. Emissivity and concentration depth distributions of acridine orange at a water/silica interface. Bulk solution concentration = 2.1×10^{-7} mol dm^{-3}; emission wavelengths = 550 nm (a, c) and 650 nm (b, d).

Figure 10 are expressed in terms of the product of the quantum yield and concentration, the emissivity). Figure 10b clearly shows that the intensity of fluorescence emission per unit volume originating within 40 nm of the surface is 20 times greater than that originating per unit volume from the bulk AO ($z > 40$ nm). Kinetic studies assigned fluorescence lifetimes of ≈25 ns for surface specific AO and 2.1 ns for bulk AO. Since k_r is unaffected by the interface, the fluorescence quantum yield of "surface-associated" AO is approximately 12 times greater than that of bulk AO. Consequently each AO molecule in the interfacial region generates 12 times the number of florescence photons than each "bulk" AO molecule. Using this information the emissivity depth distribution is converted into the more useful concentration depth distribution. This is shown in Figure 10d. This confirms that the red emission originates from a surface-specific layer (i.e. $z < 40$ nm)

A similar treatment can be performed for AO molecules emitting fluorescence at 550 nm (Figures 10a,c). Here the emissivity depth distribution shows that emission from a region within 40 nm of the surface is 1.5 times greater than that of bulk AO. However the enhancement in fluorescence quantum yield of the surface-specific species means that although the emissivity at 550 nm is increased in the interfacial region the concentration is actually depleted, Figure 10c. For AO molecules emitting fluorescence at 550 nm, the concentration in the interfacial region is 8 times less than in the bulk solution.

Conclusion

These studies have shown that VATR-EWIFS can be used to quantitatively probe the concentration depth distribution of some simple dye molecules at water/silica interfaces. It has been stressed that care must be taken when using changes in fluorescence intensities to infer changes in molecular concentration. Fortuitously, it has been demonstrated theoretically that the radiative decay rate of a fluorophore is largely uneffected by the presence of a dielectric interface (for the system described and within experimental error). This result is of great importance in quantitative EWIFS, since it allows the quantum yield of molecules in the interfacial region to be measured directly using time-resolved fluorescence measurements. Furthermore fluorescence intensities can subsequently be used to calculate molecular concentrations.

Spectral and kinetic fluorescence properties of FDSS emission appear to be uneffected by the presence of a water/silica interface. This permits a simple interpretation of angle spectra in terms of concentration distributions. Subsequent analyses of angle spectra confirm that the concentration distribution of FDSS is homogeneous as a function of distance away from the interface ($0 > z > \infty$). The absence of any specific solute−surface interactions means that FDSS is ideally suited for calibration of VATR-EWIFS measurements.

The spectral and kinetic fluorescence profiles of AO, however, illustrate a more complex system. This is evidenced by a red-shifted emission and an enhanced fluorescence lifetime of a "surface-associated" AO population. Data show that AO exists as two distinct species, "bulk" and "surface associated". The measured differences in the quantum yield allow the concentration profiles of the two species to be determined from the emissivity distributions. Conventionally these concentration distributions would have been calculated assuming the quantum yield of the "bulk" and "surface-associated" AO were identical, yielding incorrect results.[9] By spectrally selecting angle spectra from "bulk" and "surface-associated" AO populations, one can successfully test simple depth profile theory. Nevertheless, the theory can be similarly applied when the angle spectra/decays are measured using no wavelength discrimination. These studies of simple dye systems demonstrate how the multidimensionality of fluorescence can be used in conjunction with a surface-specific probe (EWIFS) to quantitatively interrogate the interfacial region.

The methodology presented here is valid for any system where a step profile is a satisfactory physical description of the concentration distribution in the interfacial region. However, it is possible and moreover likely that many systems will be more complex. Present studies of the precise behavior of AO at dielectric interfaces are combining fluorescence lifetime distribution analysis and more complex depth distribution models with VATR-EWIFS. This should provide a more complete analysis of the heterogeneous nature of many interfacial systems.

Acknowledgment. The authors thank the Engineering and Physical Sciences Research Council (EPSRC UK) for financial support. C.D.B. thanks Kodak Ltd. for an EPSRC CASE Studentship and provision of equipment.

References and Notes

(1) Lakowicz, J. R. *Principles of Fluorescence Spectroscopy*; Plenum: New York, 1983; Vols. 1−3.
(2) Lakowicz, J. R. *Topics in Fluorescence Spectroscopy*; Plenum: New York, 1991.
(3) MacRichie, F. *Chemistry at Interfaces*; Academic Press: San Diego, CA, 1990.
(4) Horbet, T. S.; Brash, J. *Proteins at Interfaces*; ACS Symposium Series; American Chemical Society: Washington, DC, 1987; Vol. 343.
(5) de Mello, A. J.; Crystal B.; Rumbles G. *J. Colloid Interface Sci.* **1994**, *169*, 161.
(6) de Mello, A. J. *Surface Analytical Techniques for Probing Biomaterial Processes*; CRC: Boca Raton, FL, 1996; Chapter 1.
(7) Toriumi, M.; Masuhara, H. *Spectrochim. Acta Rev.* **1991**, *14*, 353.
(8) Reichert, W. M. *Crit. Rev. Biocompat.* **1989**, *5*, 173.
(9) Hlady, V.; Reinecke, D. R.; Andrade, J. D. *J. Colloid Interface Sci.* **1986**, *111*, 555.
(10) Rumbles, G.; Brown, A. J.; Phillips, D. *J. Chem. Soc., Faraday Trans.* **1991**, *87*, 825.
(11) Harrick, N. J. *Internal Reflection Spectroscopy*; Interscience-Wiley: New York, 1967.
(12) Robertson, J. L.; Tilton, R. D. *Langmuir* **1996**, *12*, 6104.
(13) Watarai, H.; Funaki, F. *Langmuir* **1996**, *12*, 6717−6720.
(14) Fisher, L. *Surface analytical Techniques for Probing Biomaterial Processes*; CRC: Boca Raton, FL, 1996; Chapter 2.

(15) Masuhara, H.; Mataga, N. *Chem. Phys. Lett.* **1983**, *100*, 415.
(16) Ausserre, D.; Hervet, H.; Rondelez, F. *Macromolecules* **1986**, *19*, 9, 85.
(17) Schmid, E. L.; Tairi, A. P.; Hovius, R.; Vogel, H. *Anal. Chem.* **1998**, *70*, 1331.
(18) Asanov, A. N.; Wilson, W. W.; Oldham, P. B. *Anal. Chem.* **1998**, *70*, 1156.
(19) Gilbert, A.; Baggot, J. *Essentials of Molecular Photochemistry*; Blackwell Scientific Publications: Oxford, U.K., 1991.
(20) Bright, F. V.; Wang, R.; Lundgren, J. S. *Appl. Spectrosc. Rev.* **1997**, *32*, 1.
(21) Urbakh, M.; Klafter, J. *J. Phys. Chem.* **1992**, *96*, 3480.
(22) Urbakh, M.; Klafter, J. *J. Phys. Chem.* **1993**, *97*, 3344.
(23) Sipe, J. E. *Surf. Sci.* **1981**, *105*, 489.
(24) Yevng, M. S.; Gustafson, T. K. *Phys. Rev. A* **1996**, *54*, 5227.
(25) Chance, R. R.; Prock, A.; Silbey, R. *Adv. Chem. Phys.* **1978**, *37*, 1.
(26) Maxwell, J. C. *A Treatise on Electricity and Magnetism*; Oxford University Press: Oxford, U.K., 1873.
(27) Toriumi, M.; Masuhara, H. *Appl. Opt.* **1992**, *31*, 6376.
(28) Shick, R. A.; Koenig, J. L.; Ishida, H. *Appl. Spectrosc.* **1993**, *47*, 1237.
(29) Tompkins, G. *Appl. Spectrosc.* **1974**, *28*, 335.
(30) O'Connor, D. V.; Phillips, D. *Time-correlated Single Photon Counting*; Academic Press: San Diego, CA, 1984.
(31) Janot, J. M.; Beeby, A.; Bayiey, P. M.; Phillips, D. *Biophys. Chem.* **1991**, *41*, 277.
(32) Elmgren, H. *J. Poly. Sci., Polym. Lett. Ed.* **1980**, *18*, 815.
(33) de Mello, A. J. PhD Thesis, Imperial College, London University, 1995.
(34) James, D. R.; Ware, W. R. *Chem. Phys. Lett.* **1986**, *126*, 7.